COMMUN. MATH. SCI.
Vol. 17, No. 7, pp. 1949–1974

VARIATIONAL APPROACH TO CONCENTRATION DEPENDENT DIELECTRICS WITH THE BRUGGEMAN MODEL: THEORY AND NUMERICS*

XIANG JI† AND SHENGGAO ZHOU‡

Abstract. The structure of the electric double layer has long been described by the classical Poisson–Boltzmann (PB) theory, in which a uniform dielectric coefficient is often assumed. Experimental data and molecular simulations evidence that the effective dielectric coefficient decreases with local ionic concentrations. In this work, a variational approach is developed to incorporate nonlinear concentration-dependent dielectrics described by the Bruggeman equation in a modified PB theory. The Bruggeman equation, which takes into account contributions from both counterions and coions systematically, provides a closure to the modified PB theory. In addition to ionic size and valence, our theory introduces a new source of ion-specificity, i.e., the dielectric coefficient of hydrated ions, to the continuum modeling of electrostatics. Asymptotic analysis reveals the connection between the modified PB theory and previous linear decrement models, and derives a criterion for counterion saturation. Robust numerical methods with efficient acceleration techniques are proposed to solve the resulting coupled equations. Dielectric coefficients predicted by our theory show good agreement with the experimental data for homogeneous electrolytes. The dielectric decrement effect on the ionic structure of electric double layers is assessed in extensive numerical simulations. With ion-specific parameters, our theory predicts asymmetric camel-shape profiles of differential capacitance against applied potentials for electrolytes with low salinity, and asymmetric bell-shape profiles for electrolytes with high salinity. The impact of counterion saturation, due to steric effects or dielectric decrement, on the shape of differential capacitance profiles is demonstrated through analysis and numerical investigations. To further understand the effect of concentration-dependent dielectrics, the modified PB theory is also applied to study the distribution of counterions around charged cylinders with various dielectric coefficients.

Keywords. Concentration-dependent dielectrics; Bruggeman model; Poisson–Boltzmann theory; Differential capacitance; Contact value theorem.

AMS subject classifications. 35J20; 35J25; 35Q92; 49S05; 92C05.

1. Introduction

Understanding the structure of electric double layers (EDLs) is of interest in a wide range of areas, such as biological macromolecules, colloidal suspensions, and electrochemical devices. As a mean-field model, the Poisson–Boltzmann (PB) theory gains its popularity in describing the structure of EDLs on account of the simplicity and mathematical tractability of the models. In such models, the underlying charged system is treated as a continuum medium characterized by a dielectric coefficient. For instance, the dielectric coefficient of solutes, such as colloidal particles and biomolecules, is close to 2. In contrast, the dielectric coefficient of aqueous solvent in the classical PB-type continuum models is often set to be a homogeneous high constant, e.g., 78 [21].

The dielectric coefficient measures the polarizability of a medium in response to an external electric field. With an asymmetric molecular structure, the water molecule has large orientational polarizability, accounting for the large dielectric constant of aqueous solvent under normal conditions. However, the polarizability of solvent can be lowered pronouncedly due to the presence of charged particles, such as ions. Water molecules in the immediate proximity of ions align to the electric field generated by ions, forming

*Received: October 20, 2018; Accepted (in revised form): July 1, 2019. Communicated by Chun Liu.

†Department of Mathematics and Mathematical Center for Interdiscipline Research, Soochow University, 1 Shizi Street, Suzhou 215006, Jiangsu, China (xji@stu.suda.edu.cn).

‡Corresponding author. Department of Mathematics and Mathematical Center for Interdiscipline Research, Soochow University, 1 Shizi Street, Suzhou 215006, Jiangsu, China (sgzhou@suda.edu.cn).

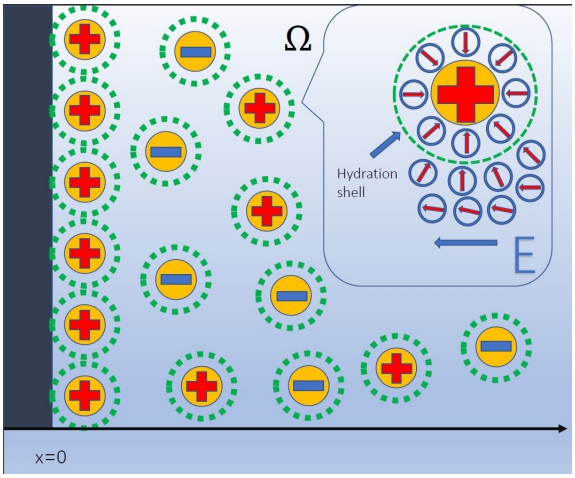

FIG. 1.1. *A schematic plot of an aqueous ionic solution in contact with a charged surface. Ions are surrounded by a layer of water molecules aligning with the local electric field created by ions. Arrows represent the orientations of dipolar water molecules.*

hydration layers; cf. Figure 1.1. The orientational polarization is much depressed for water molecules in hydration layers, leading to the phenomenon of dielectric decrement. Thus, the dielectric coefficient of electrolyte solutions are often heterogeneous, rather than a constant. Experimental data have evidenced that the dielectric coefficient should be a spatially varying function that depends on many factors related to the local environment [21,22,50,51]. For instance, nonlocal dielectric models with position-dependent dielectric permittivity have been developed to reflect permittivity correlations among solute and solvent molecules and the spatial-frequency dependence of the dielectric permittivity [2,52–54].

It is expected that the dielectric coefficient of ionic solutions decreases with ionic concentrations. Such a decrement has been confirmed by experimental data and molecular simulation results [9, 21, 22, 50, 51]. To account for the concentration-dependent dielectrics, various models have been proposed in the literature [4,5,10,15,17,18,20,30, 33,34,39–41,45]. For instance, a linear decrement model has been proposed to describe the dielectric decrement of dilute solutions [5]:

$$\varepsilon = \varepsilon_w + \gamma c, \tag{1.1}$$

where ε_w is the dielectric coefficient of water, γ is a phenomenological coefficient, and c is the ionic concentration. However, the linear decrement model gives poor prediction as the concentration goes over 1.5 M, for which the dielectric coefficient saturates due to nonlinear effects [22]. To enforce ellipticity of the Poisson's equation, the dielectric coefficient should be bounded below by a positive number. However, it is evident that the linear decrement model gives unbounded dielectric coefficient for high ionic concentrations. To include nonlinear effects, an exponential type of function with coefficients determined by fitting against experimental data has been employed to describe the effective dielectric coefficient [33]. Further analysis reveals that the corresponding free-energy functional may no longer be convex with respect to concentrations.

To take into account the contributions from both counterions and coions, the decre-

ment effects are linearly superimposed [41], i.e.,

$$\varepsilon = \varepsilon_w - \sum_{i=1}^{M} \gamma_i c_i, \tag{1.2}$$

where γ_i are ion-specific coefficients and M is the number of ionic species in the system. While the refined linear decrement model (1.2) works well for concentrations up to 1.5 M [5], ionic concentrations close to a charged surface can easily exceed 1.5 M, even for electrolytes with low bulk concentrations. The nonlinear dependence on concentrations is therefore necessary for accurate description of the structure of electric double layers. Based on a microfield approach, a nonlinear dependence of the dielectric function upon salt concentrations has been proposed for concentrated solutions [17]. The nonlinearity is taken into account with the help of the Langevin function. Recently, the dielectric coefficient is treated as a nonlinear function of the ionic strength which includes the contributions from counterions and coions together [10]. Grand canonical Monte Carlo simulations with such a concentration-dependent dielectric coefficient are able to accurately reproduce the mean ionic activity coefficients of concentrated electrolyte solutions.

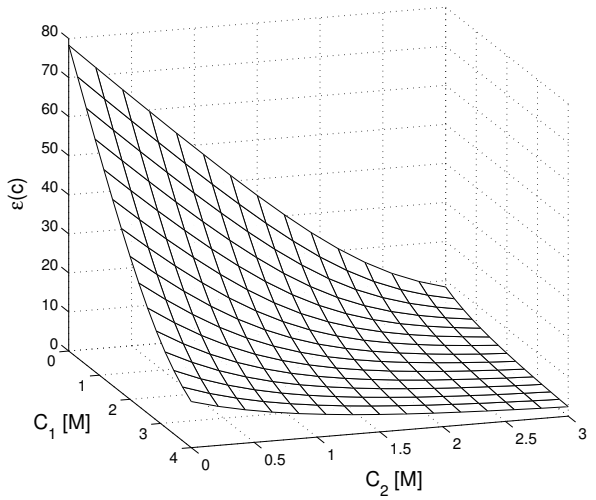

FIG. 1.2. *An illustrative plot of the effective dielectric coefficient $\varepsilon(c)$, predicted by the Bruggeman equation, as a function of ionic concentrations. There are two ion species with the parameters: $v_1 = 0.7^3\, nm^3$, $v_2 = 0.8^3\, nm^3$, $\varepsilon_w = 78$, $\varepsilon_1 = 5$, and $\varepsilon_2 = 10$.*

The Bruggeman equation in effective medium theory is a well-established model to describe the effective dielectric response of mixtures [8, 48]. It has been widely used to determine effective dielectric coefficient for heterogeneous ellipsoidal or spheroidal systems, such as polymers, energy storage capacitors, and waveguides [6, 29, 46]. In this work, we consider nonlinear dependence of dielectric coefficients on ionic concentrations through their volume fractions. For simplicity, the volume fractions of ions and solvent are defined by

$$\theta_i = v_i c_i \quad \text{and} \quad \theta_w = 1 - \sum_{i=1}^{M} \theta_i,$$

where v_i represents the volume of the i-th species of hydrated ions. The Bruggeman equation [8, 47, 48] for spherical inclusions is employed to predict the local effective dielectric coefficient, which is a nonlinear function of volume fractions and dielectric coefficients of compositions in mixtures:

$$\theta_w \frac{\varepsilon_w - \varepsilon}{\varepsilon_w + 2\varepsilon} + \sum_{i=1}^{M} \theta_i \frac{\varepsilon_i - \varepsilon}{\varepsilon_i + 2\varepsilon} = 0. \tag{1.3}$$

Here ε_i is the dielectric coefficient of the i-th species of hydrated ions. Note that $\varepsilon = \varepsilon_w$ for the case of pure water. The Bruggeman Equation (1.3) defines a nonlinear implicit function of the effective dielectric coefficient on concentrations. In contrast to previous models, the effective dielectric coefficient defined by (1.3) is able to take into account the contributions both from counterions and anions systematically, according to their volume fractions. In addition, the Bruggeman equation works for dilute cases, as well as high-concentration regimes where the linear decrement breaks down. It is of mathematical interest to note that there exist two positive numbers $\varepsilon_{\min}$ and $\varepsilon_{\max}$ such that the effective dielectric coefficient calculated by (1.3) satisfies

$$\varepsilon_{\min} \le \varepsilon(c) \le \varepsilon_{\max}.$$

This valuable property is crucial to the well-posedness of our model and robustness of numerical computations. Figure 1.2 gives an illustrative plot of the effective dielectric coefficient predicted by the Bruggeman equation, as a function of ionic concentrations. As observed in experimental data [22], the effective dielectric coefficient first decreases linearly in low-concentration regimes and gradually reaches a saturation value for high ionic concentrations.

The development of a modified Poisson–Boltzmann (PB) theory starts with a free-energy functional that takes concentration-dependent dielectrics into account. The minimization of the free-energy functional leads to governing equations of the system in equilibrium. In such a variational approach, the Bruggeman equation that determines effective dielectric coefficient through ionic concentrations and hydrated ion sizes provides a closure to the developed modified PB theory. Further analysis on the dependence of the dielectric coefficient on concentrations reveals that the linear order of the Bruggeman model presents an intuitive interpretation of the phenomenological coefficients in the linear decrement model (1.2). In addition, we derive a modified Grahame equation, from which the criterion of saturation due to dielectric decrement is established. Numerical methods with acceleration techniques are proposed to solve our model. The effect of dielectric decrement on counterion concentrations is extensively studied in numerical simulations. The simulation results on the effective dielectric coefficient give good agreement with experimental data. We also apply the developed modified PB theory to study the differential capacitance of the electric double layer capacitors. With ion-specific parameters, such as the hydrated ionic size and dielectric coefficient, our model predicts asymmetric camel-shape profiles of differential capacitance against applied potentials for electrolytes with low salinity, and asymmetric bell-shape profiles for electrolytes with high salinity. Analysis and numerical investigation demonstrate that the peaks in the asymmetric profiles correspond to the counterion saturation that arises either from steric effects or dielectric decrement. The newly introduced dielectric coefficient of hydrated ions provides a new perspective to study the asymmetry in differential capacitance profiles. The model is further applied to predict the ionic distribution around charged cylinders with various dielectric constants.

We organize the rest of the paper as follows: In Section 2, we derive governing equations by taking variation of the free-energy functional with concentration-dependent dielectrics. We analyze the properties of the Bruggeman model, and derive a modified Grahame equation. In Section 3, we propose a numerical algorithm for solving the derived governing equations. In Section 4, we present our numerical results on dielectrics, the structure of electric double layer, and differential capacitance. Finally, in Section 5, we draw our conclusions.

2. Model

2.1. Governing equations. We consider ionic solutions with M species occupying a region Ω in $\mathbb{R}^3$ with a smooth boundary $\partial\Omega$. For each i $(1\le i\le M)$, the valence of i-th species of ions is denoted by z_i, and the ionic concentration at position x is represented by $c_i(x):\Omega\to\mathbb{R}^+$. Let $c(x)=(c_1(x),\dots,c_M(x))$. To emphasize its dependence on concentrations, the effective dielectric coefficient is denoted by $\varepsilon(c):\mathbb{R}^+\to\mathbb{R}$. The electrostatic potential, denoted by $\psi:\Omega\to\mathbb{R}$, solves a boundary-value problem of the Poisson's equation:

$$\begin{cases} -\nabla\cdot\varepsilon_0\varepsilon(c)\nabla\psi=\rho(c) & \text{in }\Omega,\\ \psi=\psi_D & \text{on }\partial\Omega, \end{cases} \tag{2.1}$$

where ψ_D is a restriction of a function in $W^{2,\infty}(\Omega)$ on the boundary $\partial\Omega$. Here ε_0 is the vacuum permittivity and the effective dielectric coefficient $\varepsilon(c)$ is determined by the Bruggeman Equation (1.3) [8,47]. The charge density $\rho(c)$ is given by

$$\rho(c)=\rho^{\mathrm{f}}+\sum_{i=1}^{M}q_ic_i, \tag{2.2}$$

where the function $\rho^{\mathrm{f}}:\Omega\to\mathbb{R}$ represents the fixed charge density, and $q_i=z_ie$ with z_i the valence of the i-th ionic species and e the elementary charge. The mean-field free energy of such a charged system is given by [7,31,38]

$$\begin{aligned} F[c]=&\int_\Omega\frac{1}{2}\rho(c)\psi(c)\,dV-\int_{\partial\Omega}\frac{1}{2}\varepsilon_0\varepsilon(c)\frac{\partial\psi(c)}{\partial n}\psi_D\,dS\\ &+\beta^{-1}\sum_{i=0}^{M}\int_\Omega c_i[\log(v_ic_i)-1]\,dV-\sum_{i=1}^{M}\int_\Omega\mu_ic_i\,dV, \end{aligned} \tag{2.3}$$

where $\partial\psi(c)/\partial n$ denotes the normal derivative on $\partial\Omega$ with n the exterior unit normal, $\beta^{-1}=k_BT$ with k_B being the Boltzmann constant and T being the absolute temperature, v_i $(1\le i\le M)$ denotes the volume of a hydrated ion and v_0 is the volume of a solvent molecule, μ_i is the chemical potential of the i-th species of ions. For $i=0$, $c_0(x):\Omega\to\mathbb{R}^+$ represents the local concentration of solvent molecules and is given by

$$c_0(x)=v_0^{-1}\left[1-\sum_{i=1}^{M}\theta_i(x)\right]. \tag{2.4}$$

We here have assumed full packing of particles, whereas there are voids among nonuniform particles. To refine the packing description, the interstitial voids can be introduced as an additional particle species [35,36,54]. In these types of models, the steric effect of ions is considered by including the entropy of solvent with its concentration given by

(2.4). Other types of models that are based on the steric interactions between ions have been proposed in the literature [12, 16, 23, 25, 44, 55].

In the rest of the paper, we make the following assumptions.

(A1) The $\Omega \subset \mathbb{R}^3$ is a bounded, open, and connected domain with a smooth boundary $\partial\Omega$.

(A2) The distribution of the fixed charge density ρ^{f} is a given function with $\rho^{\mathrm{f}} \in L^\infty(\Omega)$. The boundary data ψ_D is a given function that is a restriction on $\partial\Omega$ of a function in $W^{2,\infty}(\Omega)$. For the local minimizer of the free-energy functional $c^{\mathrm{Min}}(x) := \mathrm{argmin} F[c]$, there exist positive numbers C_l and C_u such that $C_l \le c_i^{\mathrm{Min}}(x) \le \frac{1}{v_i} - C_u$ for a.e. $x \in \Omega$ and $i = 1, \ldots, M$;

(A3) The effective dielectric coefficient is a decreasing function with $\varepsilon \in C^1([0,\infty))$. The dielectric coefficients of hydrated ions satisfy $0 < \varepsilon_i < \varepsilon_w$ $(1 \le i \le M)$.

Note that we have used the standard notion for Sobolev spaces [1]. It follows from the Bruggeman Equation (1.3) that the effective dielectric coefficient satisfies

$$\mathrm{Min}(\varepsilon_1, \varepsilon_2, \ldots, \varepsilon_M) \le \varepsilon(c) \le \mathrm{Max}(\varepsilon_1, \varepsilon_2, \ldots, \varepsilon_M). \tag{2.5}$$

In the free-energy functional (2.3), the first integral term is the electrostatic potential energy, the second integral represents the entropy of ions and solvent molecules, and the last term is the contribution from the chemical potential. For simplicity, we rewrite $F[c] = F_{\mathrm{pot}}[c] + F_{\mathrm{ent}}[c] + F_{\mathrm{chem}}[c]$, where

$$F_{\mathrm{pot}}[c] = \int_\Omega \frac{1}{2}\rho(c)\psi(c)\, dV - \int_{\partial\Omega} \frac{1}{2}\varepsilon_0\varepsilon(c)\frac{\partial\psi(c)}{\partial n}\psi_D\, dS, \tag{2.6}$$

$$F_{\mathrm{ent}}[c] = \beta^{-1}\sum_{i=0}^{M}\int_\Omega c_i[\log(v_i c_i) - 1]\, dV, \tag{2.7}$$

$$F_{\mathrm{chem}}[c] = -\sum_{i=1}^{M}\int_\Omega \mu_i c_i\, dV. \tag{2.8}$$

We now perform sensitivity analysis on each ionic species to derive the variation of the free-energy functional with respect to concentrations. We consider an infinitesimally small perturbation, δc_j, to the j-th ionic concentration. Let $\delta c = (0, \ldots, \delta c_j, \ldots, 0)$. Such a perturbation in concentration in turn induces a small perturbation on the electrostatic potential $\delta\psi$. The boundary-value problem of the Poisson's Equation (2.1) has a unique weak solution ψ satisfying

$$\int_\Omega \varepsilon_0\varepsilon(c)\nabla\psi\cdot\nabla\eta\, dV = \int_\Omega \rho(c)\eta\, dV \qquad \forall \eta \in H_0^1(\Omega). \tag{2.9}$$

It follows from the Poisson's equation that

$$\int_\Omega \varepsilon_0\varepsilon(c)\nabla\psi\cdot\nabla\psi\, dV - \int_{\partial\Omega}\varepsilon_0\varepsilon(c)\frac{\partial\psi}{\partial n}\psi_D\, dS = \int_\Omega \rho(c)\psi\, dV. \tag{2.10}$$

After perturbation, we analogously have

$$\begin{aligned}&\int_\Omega \varepsilon_0\varepsilon(c+\delta c)\nabla(\psi+\delta\psi)\cdot\nabla\psi\, dV - \int_{\partial\Omega}\varepsilon_0\varepsilon(c+\delta c)\frac{\partial(\psi+\delta\psi)}{\partial n}\psi_D\, dS\\ &= \int_\Omega [\rho(c) + q_j\delta c_j]\psi\, dV.\end{aligned} \tag{2.11}$$

Keeping terms up to the linear order, we obtain from (2.9) with $\eta = \delta\psi$ and subtraction of (2.10) from (2.11) that

$$\begin{aligned}\delta F_{\text{pot}}[c] &= \frac{1}{2}\int_\Omega q_j \delta c_j \psi\, dV + \frac{1}{2}\int_\Omega q_j \delta c_j \psi\, dV - \frac{1}{2}\int_\Omega \varepsilon_0 \frac{\partial \varepsilon(c)}{\partial c_j}\delta c_j |\nabla\psi|^2\, dV \\ &= \int_\Omega \left[q_j\psi - \frac{1}{2}\varepsilon_0 \frac{\partial \varepsilon(c)}{\partial c_j}|\nabla\psi|^2\right]\delta c_j\, dV. \end{aligned} \tag{2.12}$$

The leading order perturbation of the entropic part reads

$$\delta F_{\text{ent}}[c] = \beta^{-1}\int_\Omega \left[\log(v_j c_j) - \frac{v_j}{v_0}\log\left(1 - \sum_{i=1}^M v_i c_i\right)\right]\delta c_j\, dV. \tag{2.13}$$

Similarly, we have the perturbation of the contribution from the chemical potential:

$$\delta F_{\text{chem}}[c] = -\int_\Omega \mu_j \delta c_j\, dV. \tag{2.14}$$

Combining (2.12), (2.13), and (2.14) and letting $\delta c_j \to 0$, we have the first variation of the free-energy functional with respect to each concentration:

$$\frac{\delta F[c]}{\delta c_j} = q_j\psi - \frac{1}{2}\varepsilon_0\frac{\partial\varepsilon(c)}{\partial c_j}|\nabla\psi|^2 + \beta^{-1}\left[\log(v_j c_j) - \frac{v_j}{v_0}\log\left(1 - \sum_{i=1}^M v_i c_i\right)\right] - \mu_j.$$

Thus, the chemical potential is obtained from the Euler-Lagrange equation:

$$\mu_j = q_j\psi - \frac{1}{2}\varepsilon_0\frac{\partial\varepsilon(c)}{\partial c_j}|\nabla\psi|^2 + \beta^{-1}\left[\log(v_j c_j) - \frac{v_j}{v_0}\log\left(1 - \sum_{i=1}^M v_i c_i\right)\right]. \tag{2.15}$$

At equilibrium, the chemical potential is a constant determined by bulk values, i.e.,

$$\mu_j = \beta^{-1}\left[\log(v_j c_j^\infty) - \frac{v_j}{v_0}\log\left(1 - \sum_{i=1}^M v_i c_i^\infty\right)\right]. \tag{2.16}$$

Finally, we arrive at the generalized Boltzmann distributions

$$q_j\psi - \frac{1}{2}\varepsilon_0\frac{\partial\varepsilon(c)}{\partial c_j}|\nabla\psi|^2 + \beta^{-1}\left[\log\left(\frac{c_j}{c_j^\infty}\right) - \frac{v_j}{v_0}\log\left(\frac{1 - \sum_{i=1}^M v_i c_i}{1 - \sum_{i=1}^M v_i c_i^\infty}\right)\right] = 0. \tag{2.17}$$

Denote by c_0 the characteristic concentration and $\lambda_D = \sqrt{\frac{\varepsilon_0 k_B T}{c_0 e^2}}$ the characteristic length. Introduce $\widetilde{x} = \frac{x}{\lambda_D}$, $\widetilde{c_i} = \frac{c_i}{c_0}$, $\widetilde{c_i}^\infty = \frac{c_i^\infty}{c_0}$, $\widetilde{v_i} = v_i c_0$, $\phi = \frac{e\psi}{k_B T}$, $\phi_D = \frac{e\psi_D}{k_B T}$, and $\widetilde{\rho}^{\text{f}} = \frac{\rho^{\text{f}}}{e c_0}$. Dropping the tildes in new variables, we have the following dimensionless governing equations for the electrostatic potential and concentrations at equilibrium:

$$\begin{cases} -\nabla\cdot\varepsilon(c)\nabla\phi = \rho^{\text{f}} + \sum_{i=1}^M z_i c_i \text{ in } \Omega, \text{ with } \phi = \phi_D \text{ on } \partial\Omega, \\ \theta_w \dfrac{\varepsilon_w - \varepsilon(c)}{\varepsilon_w + 2\varepsilon(c)} + \sum_{i=1}^M \theta_i \dfrac{\varepsilon_i - \varepsilon(c)}{\varepsilon_i + 2\varepsilon(c)} = 0, \\ z_j\phi - \dfrac{1}{2}\dfrac{\partial\varepsilon(c)}{\partial c_j}|\nabla\phi|^2 + \log\left(\dfrac{c_j}{c_j^\infty}\right) - \dfrac{v_j}{v_0}\log\left(\dfrac{\theta_w}{\theta_w^\infty}\right) = 0 \quad \text{for } 1 \le j \le M. \end{cases} \tag{2.18}$$

2.2. Bruggeman model. The Bruggeman Equation (1.3) calculates an effective dielectric constant for a medium that consists of multi-component spherical inclusions with different dielectric constants. We here consider the effective dielectric constant in the limits of dilute and concentrated ionic solutions with two ionic species.

In the limit of dilute solutions, the ionic concentration $c_i \to 0$ for $1 \le i \le 2$. Then the effective dielectric constant has an asymptotic expansion

$$\varepsilon(c) = \varepsilon_w + cg^T + \frac{1}{2} cGc^T + o(c^2), \tag{2.19}$$

where $o(c^2)$ are higher order terms,

$$g = \left(\frac{3\varepsilon_w(\varepsilon_w - \varepsilon_1)v_1}{\varepsilon_1 + 2\varepsilon_w}, \frac{3\varepsilon_w(\varepsilon_w - \varepsilon_2)v_2}{\varepsilon_2 + 2\varepsilon_w} \right),$$

and the Hessian matrix

$$G = \begin{bmatrix} \frac{18(\varepsilon_1 - \varepsilon_w)^2 \varepsilon_1 \varepsilon_w v_1^2}{(\varepsilon_1 + 2\varepsilon_w)^3} & g_{12} \\ g_{21} & \frac{18(\varepsilon_2 - \varepsilon_w)^2 \varepsilon_2 \varepsilon_w v_2^2}{(\varepsilon_2 + 2\varepsilon_w)^3} \end{bmatrix} \tag{2.20}$$

with cross-derivative terms

$$g_{12} = g_{21} = \frac{18\varepsilon_w v_1 v_2 (\varepsilon_w - \varepsilon_1)(\varepsilon_w - \varepsilon_2)(4\varepsilon_w + 2\varepsilon_2 + 3\varepsilon_w\varepsilon_1 + \varepsilon_w\varepsilon_2 + \varepsilon_1\varepsilon_2 - 8\varepsilon_w^2)}{(2\varepsilon_w + \varepsilon_1)(2\varepsilon_w + \varepsilon_2)(4\varepsilon_1 - 8\varepsilon_w + 4\varepsilon_2 - 2\varepsilon_w\varepsilon_1 - 2\varepsilon_w\varepsilon_2 + \varepsilon_1\varepsilon_2 + 12\varepsilon_w^2)}.$$

Such an expansion reveals that the effective dielectric constant reduces to the dielectric constant of water in the dilute limit. Also, one can see that, up to terms of linear order, the effective dielectric constant decreases linearly with respect to concentrations. Recall a linear decrement model proposed in [41]:

$$\varepsilon(c) = \varepsilon_w - \gamma_1 c_1 - \gamma_2 c_2.$$

It is not straightforward to determine the coefficients γ_i separately based on experimental data [41]. Interestingly, our model provides a physical interpretation of such two coefficients:

$$\gamma_i = \frac{3\varepsilon_w(\varepsilon_w - \varepsilon_i)v_i}{\varepsilon_i + 2\varepsilon_w}. \tag{2.21}$$

The higher order terms in c_i represent the nonlinear correction to the dielectric decrement. Although the diagonal terms of the Hessian matrix are positive, detailed calculations on the determinant of the matrix show that the matrix is indefinite. The indefiniteness of the matrix leads to a nonconvex free-energy functional (2.3) with respect to concentrations, when the solution is dilute. Interested readers are referred to the work [33] for the detailed mathematical analysis on non-convexity.

In the limit of concentrated solutions, we have $\theta_w \to 0$. The effective dielectric constant is given by

$$\varepsilon(c) \to \frac{\theta_1(2\varepsilon_1 - \varepsilon_2) + \theta_2(2\varepsilon_2 - \varepsilon_1)}{4} + \frac{\sqrt{[\theta_1(2\varepsilon_1 - \varepsilon_2) + \theta_2(2\varepsilon_2 - \varepsilon_1)]^2 + 8\varepsilon_1\varepsilon_2}}{4}, \text{ as } \theta_w \to 0.$$

When c_2 is fully depleted from the charged surface, we have the following asymptotic expansions in terms of θ_w:

$$\varepsilon(c) = \varepsilon_1 + \frac{3\varepsilon_1(\varepsilon_w - \varepsilon_1)}{\varepsilon_w + 2\varepsilon_1}\theta_w + \frac{9(\varepsilon_w - \varepsilon_1)^2\varepsilon_1\varepsilon_w}{(\varepsilon_w + 2\varepsilon_1)^3}\theta_w^2 + o(\theta_w^2). \tag{2.22}$$

It is easy to find that $\varepsilon(c) \to \varepsilon_1$, as expected.

2.3. Contact value theorem. The contact value theorem is an important conclusion that states the force balance on a planar charged surface. It is of interest to derive the conclusion with our modified PB model. We now focus on a simple system that consists of a planar charged surface connected to an electrolyte reservoir. Due to the simplicity of geometry, our model can be reduced to a one-dimensional case with the origin located at the charged surface, cf. Figure 1.1. To derive the contact value theorem, we first calculate the pressure, which satisfies [26]

$$P'(x) = \sum_{j=1}^{M} c_j(x)\mu_j'(x), \tag{2.23}$$

where the chemical potential μ_j is given by (2.15). We have by integrating the Equation (2.23) and integration by parts that

$$\begin{aligned}
P(x) - P(\infty) &= \sum_{j=1}^{M}\int_{\infty}^{x} c_j\mu_j'\,d\xi \\
&= \sum_{j=1}^{M}\int_{\infty}^{x} q_j c_j\psi' - \frac{\varepsilon_0 c_j}{2}\left[\frac{\partial\varepsilon(c)}{\partial c_j}\psi'^2\right]' + \beta^{-1}\left(c_j' + \frac{v_j c_j\sum_{i=1}^{M}\theta_i'}{v_0\theta_w}\right)d\xi \\
&= \int_{\infty}^{x} -(\varepsilon_0\varepsilon(c)\psi')'\psi'\,d\xi - \sum_{j=1}^{M}\frac{\varepsilon_0 c_j}{2}\frac{\partial\varepsilon(c)}{\partial c_j}\psi'^2\Big|_{\infty}^{x} + \int_{\infty}^{x}\frac{\varepsilon_0}{2}\sum_{j=1}^{M}c_j'\frac{\partial\varepsilon(c)}{\partial c_j}\psi'^2\,d\xi \\
&\quad + \beta^{-1}\int_{\infty}^{x}\sum_{j=1}^{M}c_j' + \frac{(1-\theta_w)\sum_{i=1}^{M}\theta_i'}{v_0\theta_w}\,d\xi,
\end{aligned}$$

where we have used the Poisson's equation. Using integration by parts twice, we have

$$\begin{aligned}
P(x) - P(\infty) &= -\varepsilon_0\varepsilon(c)\psi'^2\big|_{\infty}^{x} - \sum_{j=1}^{M}\frac{\varepsilon_0 c_j}{2}\frac{\partial\varepsilon(c)}{\partial c_j}\psi'^2\Big|_{\infty}^{x} + \int_{\infty}^{x}\frac{\varepsilon_0}{2}\sum_{j=1}^{M}c_j'\frac{\partial\varepsilon(c)}{\partial c_j}\psi'^2\,d\xi \\
&\quad + \frac{\varepsilon_0}{2}\int_{\infty}^{x}\varepsilon(c)d\psi'^2 + \beta^{-1}\left[\sum_{i=1}^{M}c_i - \frac{1}{v_0}(\log\theta_w - \theta_w)\right]\Big|_{\infty}^{x} \\
&= -\frac{\varepsilon_0}{2}\left[\varepsilon(c) + \sum_{i=1}^{M}c_i\frac{\partial\varepsilon(c)}{\partial c_i}\right]\psi'^2\Big|_{\infty}^{x} + \beta^{-1}\left[\sum_{i=1}^{M}c_i - \frac{1}{v_0}(\log\theta_w - \theta_w)\right]\Big|_{\infty}^{x}.
\end{aligned}$$

Thus, the pressure at location x is given by

$$P(x) = -\frac{\varepsilon_0}{2}\left[\varepsilon(c) + \sum_{i=1}^{M}c_i\frac{\partial\varepsilon(c)}{\partial c_i}\right]\psi'^2 + \beta^{-1}\left\{\sum_{i=0}^{M}c_i - \frac{1}{v_0}\log\theta_w\right\}. \tag{2.24}$$

Note that the pressure is consistent with the classical PB case if the ionic volumes go to zero and the dielectric coefficient is independent of ionic concentrations. At equilibrium, the pressure is a constant for all x. By $P(0)=P(\infty)$, we have a modified Grahame equation

$$\frac{\sigma^2}{2\varepsilon_0\varepsilon(c^s)^2}\left[\varepsilon(c^s)+\sum_{i=1}^{M}c_i^s\frac{\partial\varepsilon(c^s)}{\partial c_i}\right]=\beta^{-1}\left[\sum_{i=0}^{M}(c_i^s-c_i^\infty)-\frac{1}{v_0}\log\left(\frac{\theta_w^s}{\theta_w^\infty}\right)\right], \tag{2.25}$$

where the superscript s represents the value at the surface.

2.4. Counterion saturation. Near a highly charged surface, the counterions are strongly attracted to the surface due to electrostatic interactions. It is known that the ionic steric effect hinders the counterion accumulation and gives rise to counterions saturation at the surface [4, 7, 28, 31, 32, 57]. As counterions saturate at close packing, its concentration can be estimated by $1/v$ with v being the volume of counterions. In addition to the steric effect, the dielectric decrement depletes the counterions near the charged surface as well [5, 20, 33, 41]. The interplay between these two mechanisms and their influences on the structure of the electric double layer have been elaborated with a linear dielectric decrement model [41]. We now investigate the distribution of counterions under the influence of both the steric effect and dielectric decrement described by the Bruggeman equation, and characterize the condition for which the effect becomes predominant.

We assume that there are two ionic species in the ionic solution ($M=2$). When counterions saturate at the charged surface, it is reasonable to assume that the coions, c_2, are fully depleted from the charged surface. The modified Grahame Equation (2.25) reduces to

$$\sigma^2\approx\frac{2\beta^{-1}\varepsilon_0\varepsilon(c^s)^2}{\varepsilon(c^s)+c_1^s\frac{\partial\varepsilon(c^s)}{\partial c_1}}\left[(c_1^s-c_1^\infty)-\frac{1}{v_0}\log\left(\frac{1-v_1c_1^s}{1-v_1c_1^\infty}\right)\right]. \tag{2.26}$$

Define

$$\varepsilon_d(c^s)=\varepsilon(c^s)+c_1^s\frac{\partial\varepsilon(c^s)}{\partial c_1}.$$

Solving the Bruggeman Equation (1.3), we obtain

$$\varepsilon_d=\frac{2\varepsilon_w-\varepsilon_1+2\phi_c}{4}+\frac{\sqrt{(2\varepsilon_w-\varepsilon_1+\phi_c)^2+8\varepsilon_1\varepsilon_w}}{4}+\frac{\phi_c(2\varepsilon_w-\varepsilon_1+\phi_c)}{4\sqrt{(2\varepsilon_w-\varepsilon_1+\phi_c)^2+8\varepsilon_1\varepsilon_w}}, \tag{2.27}$$

where $\phi_c=3v_1c_1^s(\varepsilon_1-\varepsilon_w)$. Since the counterion concentration at the surface is higher than that in the bulk, the Equation (2.26) implies that $\varepsilon_d>0$. Detailed calculations show that such an inequality is equivalent to

$$\phi_c>\frac{(\varepsilon_1+2\varepsilon_w)^2}{2(\varepsilon_1-2\varepsilon_w)}, \tag{2.28}$$

which gives a saturation concentration for counterions due to dielectric decrement:

$$c_1^s<\frac{(\varepsilon_1+2\varepsilon_w)^2}{6v_1(\varepsilon_1-2\varepsilon_w)(\varepsilon_1-\varepsilon_w)}. \tag{2.29}$$

Notice that the saturation due to dielectric decrement, described by the Bruggeman model, depends on both the dielectric coefficient and volume of counterions. In contrast, saturation concentration described by linear dielectric decrement is given by $c_1^s < \frac{2\varepsilon_w}{\gamma_1}$ [41]. The nonlinear dielectric decrement in the Bruggeman model accounts for such a difference in saturation concentrations.

Since both steric effects and dielectric decrement give rise to counterion saturations, we now discuss which mechanism would become predominant in determining counterion distribution. Comparing the saturation concentrations induced by two mechanisms, (2.29) versus $c_1 \le 1/v_1$, we know that the dielectric decrement prevails if

$$\frac{(\varepsilon_1+2\varepsilon_w)^2}{6(\varepsilon_1-2\varepsilon_w)(\varepsilon_1-\varepsilon_w)}<1,$$

which is equivalent to

$$\varepsilon_1 < \frac{2}{5}\varepsilon_w.$$

Otherwise, the counterions close to the highly charged surface are constrained by the steric effect with the saturation concentration $1/v_1$. Analysis here shows that $\frac{2}{5}\varepsilon_w$ is a critical threshold value for counterions to distinguish the predominance of steric effects from the dielectric decrement. Counterion saturation is further numerically studied in Section 4.2.

3. Numerical methods

We present our numerical methods in a 2D rectangular domain $\Omega=(a,b)\times(c,d)$. We introduce grid points

$$a=x_1<x_2<\cdots<x_{N_x}=b,$$
$$c=y_1<y_2<\cdots<y_{N_y}=d,$$

where N_x and N_y are the number of grid points along each dimension. Define

$$x_{i+\frac{1}{2}}=\frac{x_i+x_{i+1}}{2} \quad \text{and} \quad y_{j+\frac{1}{2}}=\frac{y_j+y_{j+1}}{2} \quad \text{for } i=1,\dots,N_x-1,\ j=1,\dots,N_y-1.$$

The domain is covered by a nonuniform mesh

$$\{x_i,y_j\} \quad \text{for } i=1,\dots,N_x,\ j=1,\dots,N_y,$$

with grid spacing given by

$$h_i^x=x_{i+\frac{1}{2}}-x_{i-\frac{1}{2}},\ h_j^y=y_{j+\frac{1}{2}}-y_{j-\frac{1}{2}} \text{ for } i=1,\dots,N_x-1,\ j=1,\dots,N_y-1,$$

and

$$h_{i+\frac{1}{2}}^x=x_{i+1}-x_i,\ h_{j+\frac{1}{2}}^y=y_{j+1}-y_j \text{ for } i=1,\dots,N_x-1,\ j=1,\dots,N_y-1.$$

We denote by $c_{i,j}^l$, $\phi_{i,j}$, and $\varepsilon_{i,j}$ the numerical approximations of $c_l(x_i,y_j)$, $\phi(x_i,y_j)$, and $\varepsilon(c_1(x_i,y_j),\cdots,c_M(x_i,y_j))$, respectively. Here the index $1\le l\le M$ is used to label the ionic species. To facilitate the presentation, we introduce discrete difference operators

$$D_x^+ f_{i,j}=\frac{f_{i+1,j}-f_{i,j}}{h_{i+\frac{1}{2}}^x}, \quad D_y^+ f_{i,j}=\frac{f_{i,j+1}-f_{i,j}}{h_{j+\frac{1}{2}}^y}$$

for a grid function $f_{i,j}$ defined on grid points (x_i,y_j).

3.1. Bruggeman equation. Given the concentrations $c=(c_1,\dots,c_M)$, the effective dielectric coefficient $\varepsilon(c)$ can be obtained by numerically solving the Bruggeman Equation (1.3). It is easy to show that there exists at least one solution in the interval $[\mathrm{Min}(\varepsilon_1,\dots,\varepsilon_M),\mathrm{Max}(\varepsilon_1,\dots,\varepsilon_M)]$. Multiple solutions are possible when the number of ionic species gets large. Although multiple solutions to the Bruggeman equation could exist in the interval, it is nontrivial to prove that there exist multiple solutions of physical significance to the whole system (2.18). Existence and multiplicity of solutions to the model and related physical phenomena deserve further studies.

It is crucial to observe that the functional dependence of the effective dielectric coefficient on concentrations can be precomputed and stored before solving the coupled system (2.18). Furthermore, it follows from the constraint (2.4) that the concentration c_i ranges from zero to $\frac{1}{v_i}$. We introduce a mesh for each species of concentration

$$0=p_1^l<p_2^l<\cdots<p_{N_l}^l=\frac{1}{v_l}\quad\text{for } l=1,\dots,M, \tag{3.1}$$

where N_l is the total number of grid points for the l-th ionic species. Uniform meshes for concentrations are used in our numerical computations. Define

$$f(\varepsilon)=\theta_w(\varepsilon_w-\varepsilon)\prod_{i=1}^{M}(\varepsilon_i+2\varepsilon)+\sum_{i=1}^{M}\left[\theta_i(\varepsilon_i-\varepsilon)(\varepsilon_w+2\varepsilon)\prod_{j\neq i}^{M}(\varepsilon_j+2\varepsilon)\right].$$

For any grid point $c=\left(p_{i_1}^1,p_{i_2}^2\dots,p_{i_M}^M\right)$ $(1\le i_l\le N_l)$, we solve for an effective dielectric coefficient a scalar equation $f[\varepsilon(p_{i_1}^1,p_{i_2}^2\dots,p_{i_M}^M)]=0$ by Newton's iterations

$$\varepsilon^{k+1}=\varepsilon^k-\frac{f(\varepsilon^k)}{f'(\varepsilon^k)},$$

with an initial guess $\varepsilon^0=\varepsilon_w$. After convergence, we store $\varepsilon(p_{i_1}^1,p_{i_2}^2\dots,p_{i_M}^M)$ on the grid points (3.1). In addition, we use finite-difference schemes to compute

$$\frac{\partial\varepsilon(p_{i_1}^1,p_{i_2}^2\dots,p_{i_M}^M)}{\partial c_l}\approx\frac{\varepsilon(p_{i_1}^1,\dots,p_{i_l+1}^l,\dots,p_{i_M}^M)-\varepsilon(p_{i_1}^1,\dots,p_{i_l-1}^l,\dots,p_{i_M}^M)}{p_{i_l+1}^l-p_{i_l-1}^l}\quad\text{for } l=1,\dots,M.$$

Again, such partial derivatives are stored for each grid point. We remark that this approach gets memory demanding when the number of ion species gets large.

For any concentration $c=(c_1,\dots,c_M)$, we use high-order interpolation schemes to compute the $\varepsilon(c)$ and $\frac{\partial\varepsilon(c)}{\partial c_l}$ based on the stored data. Such a pre-computation technique can efficiently speed up the computation, especially in three dimensional calculations for applications of practical interest.

3.2. Poisson's equation. Ionic concentrations often have large variations near charged surfaces; therefore, the effective dielectric coefficient that depends on ionic concentrations may have large variations as well. Furthermore, the dielectric coefficient is often discontinuous across the dielectric interface that separates different dielectric media. We develop numerical methods for the Poisson's equation with special treatments for dielectric jump on the interface. Also, we consider Dirichlet boundary conditions on the outer boundaries of the rectangular domain with boundary data that are maintained by electrodes.

Given numerical solutions of concentrations $c^l_{i,j}$ and the corresponding $\varepsilon_{i,j}$, we discretize the Poisson's Equation (2.1) with a central differencing scheme

$$-\left(\frac{\varepsilon_{i+\frac{1}{2},j}D^+_x\phi_{i,j}-\varepsilon_{i-\frac{1}{2},j}D^+_x\phi_{i-1,j}}{h^x_i}+\frac{\varepsilon_{i,j+\frac{1}{2}}D^+_y\phi_{i,j}-\varepsilon_{i,j-\frac{1}{2}}D^+_y\phi_{i,j-1}}{h^y_j}\right)$$
$$=\rho^{\mathrm{f}}_{i,j}+\sum_{l=1}^{M}z_l c^l_{i,j}, \tag{3.2}$$

where the dielectric coefficient on the half-grid points are approximated by the harmonic mean

$$\varepsilon_{i+\frac{1}{2},j}=\frac{\varepsilon_{i,j}\varepsilon_{i+1,j}}{\omega_1\varepsilon_{i+1,j}+\omega_2\varepsilon_{i,j}}.$$

Here the weights satisfy $\omega_1\geq 0$, $\omega_2\geq 0$, and $\omega_1+\omega_2=1$. If there is no dielectric interface between grid points (i,j) and $(i+1,j)$, we simply choose $\omega_1=\omega_2=0.5$. When there is a dielectric interface, ω_1 and ω_2 are chosen according to the ratios of the distance of the interface point to adjacent grid points (i,j) and $(i+1,j)$ over $h^x_{i+\frac{1}{2}}$. Other dielectric coefficients $\varepsilon_{i-\frac{1}{2},j}$ and $\varepsilon_{i,j\pm\frac{1}{2}}$ are treated analogously. Compared to the arithmetic mean, the harmonic mean gives a smoother approximation of the dielectric coefficient and improves the accuracy of the approximation of the electrostatic potential, especially when the dielectric coefficient has large variations [11].

3.3. Generalized Boltzmann distribution. After solving the Poisson's equation, we obtain the numerical solutions of $\phi_{i,j}$ and

$$|\nabla\phi|^2_{i,j}\approx\left(\frac{\phi_{i+1,j}-\phi_{i-1,j}}{h^x_{i+\frac{1}{2}}+h^x_{i-\frac{1}{2}}}\right)^2+\left(\frac{\phi_{i,j+1}-\phi_{i,j-1}}{h^y_{j+\frac{1}{2}}+h^y_{j-\frac{1}{2}}}\right)^2.$$

Given $\phi_{i,j}$ and $|\nabla\phi|^2_{i,j}$, we update the ionic concentration by solving the generalized Boltzmann distribution (2.17), which can be reformulated as follows:

$$c_l(\theta_w,c)=c^\infty_l\exp\left[-z_l\phi+\frac{1}{2}\frac{\partial\varepsilon(c)}{\partial c_l}|\nabla\phi|^2\right]\left(\frac{\theta_w}{\theta^\infty_w}\right)^{\frac{v_l}{v_0}}\quad\text{for } 1\leq l\leq M. \tag{3.3}$$

We remark that the above equations are spatially decoupled for each grid point. However, concentrations c_l for $1\leq l\leq M$ are still coupled. We define

$$h(\theta_w,c)=\theta_w+\sum_{i=1}^{M}v_i c^\infty_i\exp\left[-z_i\phi+\frac{1}{2}\frac{\partial\varepsilon(c)}{\partial c_i}|\nabla\phi|^2\right]\left(\frac{\theta_w}{\theta^\infty_w}\right)^{\frac{v_i}{v_0}}-1. \tag{3.4}$$

It is readily verified that θ_w solves the equation $h(\theta_w,c)=0$. In the following, we propose a Newton-type iterative method to solve (3.3) on a spatial grid point (x_i,y_j).

Algorithm 1

Step 1. Given $\phi_{i,j}$ and $|\nabla\phi|^2_{i,j}$, initialize c^0 and θ^0_w. Let $k=0$. Set a stepsize $\nu\,(0<\nu<1)$.

Step 2. Update $c^{k+1}_l(\theta^k_w,c^k)$ using (3.3) with a projection on the interval $(0,1/v_l)$ for $1\leq l\leq M$.

Step 3. Update θ_w^{k+1} by Newton's iteration

$$\theta_w^{k+1} = \theta_w^k - \nu \frac{h(\theta_w^k, c^{k+1})}{\partial_{\theta_w} h(\theta_w^k, c^{k+1})},$$

with a projection on the interval $(0,1)$.

Step 4. Check convergence. If yes, the algorithm stops; otherwise, go back to Step 2.

We remark that θ_w is used as an iteration variable in the iterations, instead of c_i which have M variables. This treatment saves memory and computational time in calculations. In the iterations for θ_w, the concentrations c_l have to be updated alternatively with (3.3). It is of importance to remark that, when the linear dielectric decrement model or concentration-independent dielectrics is considered, the proposed algorithm becomes a classical Newton's method for one variable θ_w. Because the function h does not depend on concentrations in that case. With the obtained θ_w, the concentrations can be evaluated directly from (3.3). Thus, our algorithm is promising in solving other modified PB theories efficiently.

We now summarize the whole algorithm as follows:

Algorithm 2

Step 1. Initialize $k=0$ and $c^0=(c_1^0,\cdots,c_M^0)$. Set a relaxation parameter $\tau\,(0<\tau<1)$ and convergence tolerance ϵ_{tol}.

Step 2. Solve the Bruggeman Equation (1.3) for $\varepsilon(c^k)$ and $\frac{\partial\varepsilon(c^k)}{\partial c_i}\,(1\le i\le M)$; cf. Section 3.1.

Step 3. Update ϕ^{k+1} by solving the Poisson's equation with c^k and the updated $\varepsilon(c^k)$; cf. Section 3.2.

Step 4. Obtain $c^{k,*}$ by solving (3.3) with ϕ^{k+1}, $\left|\nabla\phi^{k+1}\right|$, and $\frac{\partial\varepsilon(c^k)}{\partial c_i}$; cf. Section 3.3.

Step 5. Update c^{k+1} by $c^{k+1}=\tau c^{k,*}+(1-\tau)c^k$.

Step 6. Check convergence $\text{Max}_{1\le i\le M}\|c_i^{k+1}-c_i^k\|_\infty<\epsilon_{\text{tol}}$. If yes, the algorithm stops; otherwise, go back to Step 2.

Note that the relaxation step (Step 5) with a relatively small τ is helpful in achieving final convergence.

4. Results

For simplicity of presentation, we introduce the following abbreviations in the rest of this paper:

(1) The classical Poisson–Boltzmann model is denoted by "PB".

(2) The Poisson–Boltzmann model with size effect [4, 7, 31] is denoted by "SMPB", which means the size modified PB model.

(3) Our current model with the dielectric decrement described by the Bruggeman model is denoted by "SDMPB", which means the size and dielectric modified PB model.

Note that the SMPB model can be regarded as a special case of the current SDMPB model with a uniform dielectric coefficient, i.e., $\varepsilon_i=\varepsilon_w$. To understand the effect of dielectric decrement, we also solve the classical PB model and SMPB model for comparison. Unless stated otherwise, we consider monovalent electrolytes with two ionic species. The dielectric coefficient for water is set to be $\varepsilon_w=78.3$. In the following simulations, the numerical iterations converge robustly with the choice of $\tau=0.2$.

4.1. Dielectrics.

Experiments and molecular dynamics (MD) studies have

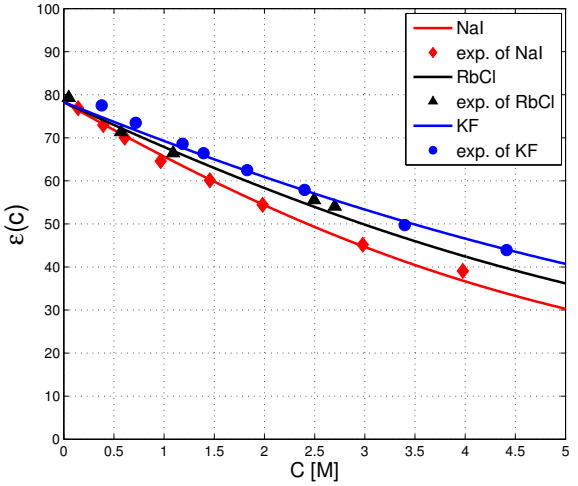

FIG. 4.1. *Comparison of predicted dielectric coefficient from the Bruggeman model (lines) and experimental data (symbols) against concentrations of different electrolyte solutions.*

evidenced that the dielectric coefficient decreases as local ionic concentrations increase [21,22,50,51]. We numerically solve the Bruggeman Equation (1.3) to investigate the dependence of dielectric coefficient on the ionic concentrations of salt solutions: NaI, RbCl, and KF. Experimental data of the dependence of dielectric coefficient on concentrations have been reported for such salt solutions in the literature [9,17,30,50]. Since the dielectric coefficients of hydrated ions are not available in the literature, we treat them as fitting parameters. In our computation, the effective hydrated ionic volume is obtained from the work [42]: $v_{Na^+} = 0.716^3\,\text{nm}^3$, $v_{I^-} = 0.662^3\,\text{nm}^3$, $v_{Rb^+} = 0.658^3\,\text{nm}^3$, $v_{Cl^-} = 0.664^3\,\text{nm}^3$, $v_{K^+} = 0.662^3\,\text{nm}^3$, and $v_{F^-} = 0.704^3\,\text{nm}^3$. Fitting against the experimental data gives the dielectric coefficient of hydrated ions: $\varepsilon_{Na^+} = 46$, $\varepsilon_{I^-} = 50$, $\varepsilon_{Rb^+} = 51$, $\varepsilon_{Cl^-} = 50$, $\varepsilon_{K^+} = 56$, and $\varepsilon_{F^-} = 55$. With these parameters, the predicted dielectric coefficients against concentrations are shown in solid lines in Figure 4.1. One can observe that, when the ionic concentrations are dilute, the dielectric decrement is linear with different slopes for different salt solutions. In addition, our theoretical prediction from the Bruggeman model agrees with the experimental data very well, even for concentrations up to 4 to 5 M. In such a high-concentration regime, the linear dielectric decrement model breaks down. The nice agreement for high concentrations indicates that the Bruggeman model is capable of capturing the dependence of the dielectric coefficient on concentrations in both low- and high-concentration regimes.

4.2. Electric double layer structure. We now apply our SDMPB model to study the effect of dielectric decrement on the ionic structure in an electric double layer (EDL). In our computations, we prescribe a fixed potential at the surface, $\psi = -10$ (in k_BT/e), as a Dirichlet boundary condition for the Poisson's equation. Also, we take the following parameters: $v_1 = 0.662^3\,\text{nm}^3$, $v_2 = 0.664^3\,\text{nm}^3$, $\varepsilon_1 = 10$, $\varepsilon_2 = 20$, and $c_{1,2}^{\infty} = 0.1M$.

As displayed in Figure 4.2, counterions are attracted to the surface due to the electrostatic interaction. With ions described by point charges, the classical PB theory

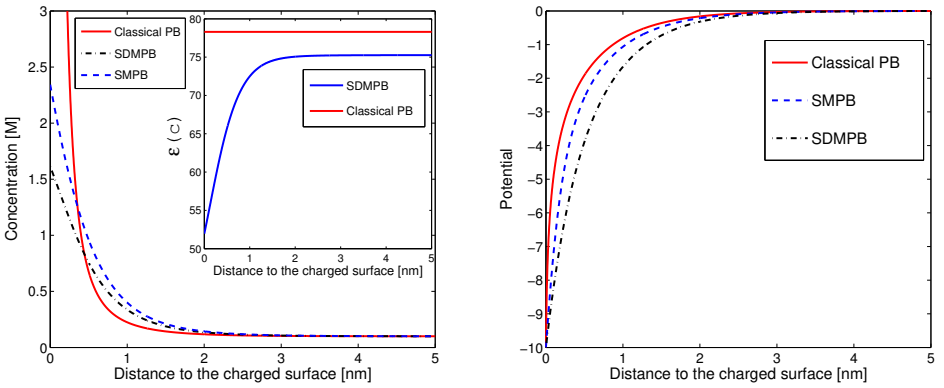

FIG. 4.2. *Left: Counterion concentrations against the distance to the charged surface for the classical PB, SMPB, and SDMPB models. The inset shows the corresponding dielectric coefficient for the classical PB and SDMPB models. Right: The electrostatic potential against the distance to the charged surface.*

predicts very high concentration at the surface. In contrast, the counterion concentration calculated by the SMPB model is much lower, as the size effect hinders counterions from accumulating at the surface. Further, when the dielectric decrement is taken into account, our SDMPB model predicts even lower concentrations. From the inset plot of Figure 4.2, one can see that the dielectric coefficient quickly decreases in the vicinity of the surface, in contrast to the case of the classical PB or SMPB that uses a uniform dielectric coefficient. Such a dielectric inhomogeneity accounts for the depletion of ions close to the surface [5, 33, 41]. The right plot of Figure 4.2 depicts the profiles of electrostatic potential obtained with different models. Because of the attracted counterions at the surface, the electrostatic potential obtained by different models gets screened quickly. Nevertheless, the potential predicted by SDMPB is screened relatively slower due to less accumulated counterions in the electric double layer. Our calculations evidence that the dielectric decrement plays a significant role in determining the structure of electric double layer.

To further understand the effect of dielectric decrement, we consider the distribution of counterions with different bulk concentrations. We use the same parameters as previous simulations, except that c_1^∞ varies from 0.1M to 1.5M. As depicted in Figure 4.3, the counterion concentration close to the surface increases as the bulk concentration goes from 0.1M to 1.5M. Of interest is that the counterion concentration becomes a non-monotone function against the distance to the surface, due to the ion depletion arising from dielectric decrement close to the surface. The equilibrium distribution of counterions reflects the competition between the electrostatic attraction and depletion from the size effect and dielectric decrement. In the immediate vicinity of the surface, the ion depletion starts to prevail over electrostatic attraction as the bulk concentration goes over a threshold value. Similar non-monotone distributions of counterions have been observed in Monte Carlo studies using concentration-dependent dielectric coefficients [20]. From the right plot of Figure 4.3, one observes that the dielectric coefficient decreases with higher counterion concentrations. As expected from the Bruggeman equation, the non-monotonicity presents itself in the distribution of dielectric coefficient as well, when $c_1^\infty = 1.5M$. As discussed in Section 2.4, there is a saturation concen-

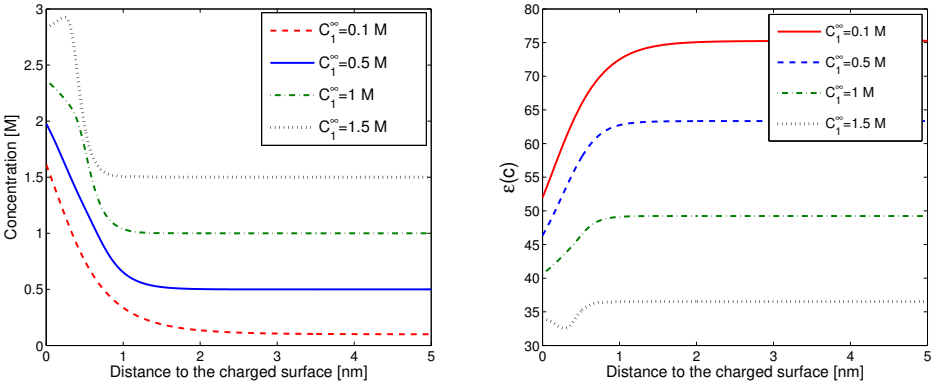

FIG. 4.3. *Left: Counterion concentrations against the distance to the charged surface. Right: Profiles of dielectric coefficient against the distance to the charged surface. The bulk counterion concentrations vary from* $0.1\,M$ *to* $1.5\,M$.

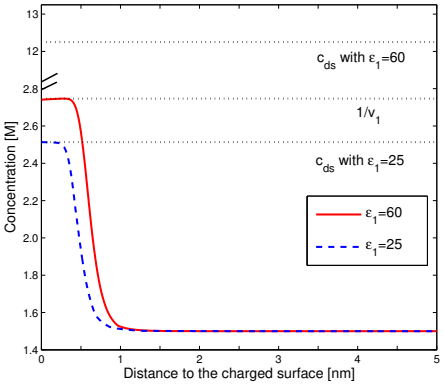

FIG. 4.4. *Counterion concentration against the distance to the surface for counterions with different dielectric coefficients* ε_1. *Saturation concentrations due to size effect or dielectric decrement are shown for reference. Notice that there is a break in the y axis.*

tration for counterions near the charged surface, if the electrostatic attraction between the surface and couterions is strong. There are two mechanisms accounting for the saturation: close packing due to size effect and dielectric decrement. In-depth analysis has demonstrated that the dielectric decrement would be predominant if the dielectric coefficient of counterions $\varepsilon_1 < \frac{2}{5}\varepsilon_w$; otherwise, the size effect prevails with the saturation concentration $1/v_1$. From (2.29), we know that the saturation concentration is given by

$$c_{\rm ds} = \frac{(\varepsilon_1 + 2\varepsilon_w)^2}{6v_1(\varepsilon_1 - 2\varepsilon_w)(\varepsilon_1 - \varepsilon_w)}.$$

We now perform two series of numerical simulations to confirm our analysis. The simulation takes the following parameters: $v_1 = 0.85^3\,\text{nm}^3$, $v_2 = 0.8^3\,\text{nm}^3$, $\varepsilon_2 = 20$, $c_{1,2}^{\infty} =$ 1.5 M, and $\psi = -10$ (in k_BT/e) at the surface. For ε_1, we take two different values:

$\varepsilon_1 = 25$ ($\varepsilon_1 < \frac{2}{5}\varepsilon_w$) and $\varepsilon_1 = 60$ ($\varepsilon_1 > \frac{2}{5}\varepsilon_w$).

Figure 4.4 shows the profiles of counterion concentrations with two different ε_1 values. For reference, the saturation concentrations due to size effect and dielectric decrement are shown as well. For $\varepsilon_1 = 60$, one can see that there is an extended condensed layer of counterions with a saturation concentration, $1/v_1$, due to the size effect, while the saturation concentration due to dielectric decrement is much higher. For $\varepsilon_1 = 25$, the saturation concentration due to dielectric decrement becomes lower than the constraint by size effect, and the concentration in the vicinity of the surface reaches the saturation concentration due to dielectric decrement. Such simulation results corroborate our analysis on the competition between two mechanisms.

4.3. Differential capacitance. The structure of a charged surface and ions adsorbed in electric double layers (EDLs) is analogous to conventional dielectric capacitors with an inter-electrode separation about the radius of a counterion. Due to the small separation, such electric double layer capacitors often can achieve very large capacitance values. As discussed in the previous section, counterions saturate in the vicinity of charged surface on account of finite ionic sizes and dielectric decrement. Wider EDLs, resulting from counterion saturation, have lower differential capacitance values [41]. We here discuss the impact of steric effect and dielectric decrement on the value of EDL differential capacitance.

4.3.1. Comparison of modified PB models. We consider the differential capacitance of an EDL with the following parameters: $z_1 = +1$, $z_2 = -1$, and $c_1^\infty = c_2^\infty = 0.1$ M. Figure 4.5 displays curves of differential capacitance against the applied surface potential that varies from -10 to 10 k_BT/e. Four different theoretical models are used to predict the differential capacitance at given surface potential. The classical PB theory predicts a monotonically increasing curve when the strength of surface potential increases. Since ions are modeled as point charges in the classical PB theory, more energy is stored in the EDL layer with more counterions piling up at the surface without steric hindrance. As the surface potential increases, the differential capacitance diverges exponentially, being consistent with the formula for the classical PB theory [3].

In contrast, the differential capacitance predicted by the SMPB models first increases with the strength of surface potential, but decreases after the surface potential exceeds a certain threshold value. Such a non-monotone dependence gives a camel-shape curve, which has been seen in experimental studies [3]. The decline of differential capacitance can be ascribed to the growth in the width of effective EDL capacitor arising from counterion saturation [28, 41, 43]. Notice that the differential capacitance curve is symmetric when uniform ionic sizes are used in the simulation, cf. the blue dash-dot line shown in Figure 4.5. Nevertheless, the curve becomes asymmetric if non-uniform ionic sizes are used. For instance, the cation is the counterion to the surface with a negative potential. Since the size of cations does not change in simulations, the curves with negative potentials overlap for the SMPB model with symmetric or asymmetric sizes, cf., the green and blue curves in the figure. This indicates that the size of coions has very limited effect on the differential capacitance. In contrast, the curves behave differently when the potential becomes positive. Because anions become counterions to the surface, and the size of anions has changed from 0.4^3 to $0.5^3\,\mathrm{nm}^3$. With larger counterion sizes, the differential capacitance becomes smaller, as less charges are stored in the EDLs.

From the black solid curve, one can observe that the differential capacitance decreases further with the inclusion of dielectric decrement. As discussed before, the saturation due to dielectric decrement prevails over the steric effect when $\varepsilon_i < \frac{2}{5}\varepsilon_w$. From the

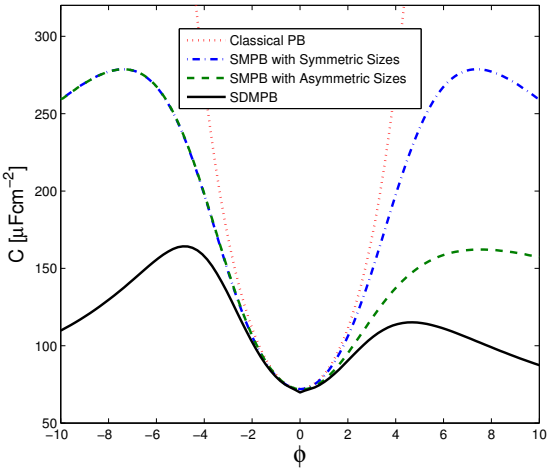

FIG. 4.5. *Differential capacitance versus surface potential predicted by different models. The red dotted line is calculated by the classical PB theory. The blue dash-dot line is calculated by the SMPB model with uniform ionic sizes ($v_1 = v_2 = 0.4^3\, nm^3$). The green dashed line corresponds to the SMPB model with nonuniform ionic sizes ($v_1 = 0.4^3\, nm^3$ and $v_2 = 0.5^3\, nm^3$). The black solid line represents the SDMPB model with parameters: $v_1 = 0.4^3\, nm^3$, $v_2 = 0.5^3\, nm^3$, $\varepsilon_1 = 10$, and $\varepsilon_2 = 20$.*

parameters used here, we know that the saturation due to dielectric decrement occurs, both for cations and anions, as the surface potential exceeds certain strength. In addition, as estimated by the Equation (2.29), the saturation concentration corresponding to cations and anions has a ratio: $c_{\mathrm{ds}}^{+1} : c_{\mathrm{ds}}^{-1} = 1.38 : 1$. This is consistent with the two peaks in the curve that the peak value of differential capacitance is higher when the surface potential is negative. Because more cations are crowding at the surface when the potential is negative. Such asymmetric differential capacitance curves evidence that our SDMPB model can effectively capture the ion-specificity, such as the ionic volume and dielectric response of hydrated ions.

4.3.2. Camel shape to bell shape. The dependence of differential capacitance on the surface potential exhibits a camel-shape curve at low salinity. Such a shape has also been observed in Monte Carlo simulations [13] and experimental studies [19, 28]. As the bulk concentration increases, the capacitance-potential curve changes from a camel shape to a bell shape, which has also been observed in experiments of ionic liquids [28,41]. We now apply our model to probe the effect of the bulk concentration on the capacitance-potential curves. Figure 4.6 presents the capacitance-potential curves with bulk concentrations ranging from 0.01 to 2 M. From Section 4.2, we know that the threshold potential for counterion saturation lowers when the bulk concentration increases. Therefore, the two peaks in the camel-shape curve get close when the bulk concentration increases, gradually switching from a camel shape to a bell shape that has a single peak at the center. At high salinity, e.g., $c_1^{\infty} = 2$ M, the nonlinear dielectric decrement described by the Bruggeman model becomes more and more important, and the curve becomes asymmetric, with the main capacitance peak slightly shifting to a positive surface potential. The effect of size and dielectric disparity on the differential capacitance predicted from our model qualitatively agrees well with Density Functional Theory (DFT) [27] and MD simulations [14].

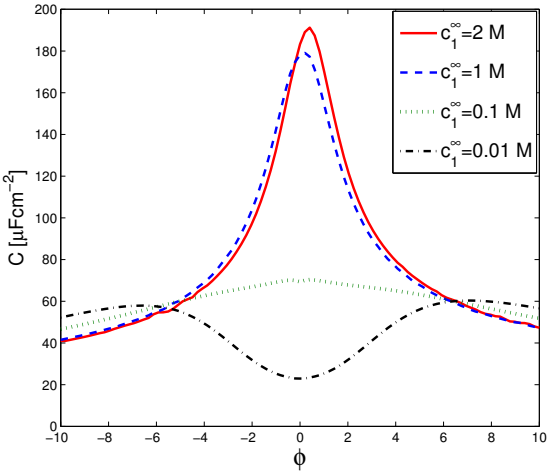

FIG. 4.6. *Differential capacitance versus surface potential using various bulk concentrations. The simulations use the parameters:* $v_1 = 0.662^3\, nm^3$, $v_2 = 0.664^3\, nm^3$, $\varepsilon_1 = 10$, *and* $\varepsilon_2 = 20$.

4.3.3. Effect of Ion-specific parameters. To further understand asymmetric capacitance-potential curves, we investigate the differential capacitance with different counterion volumes, dielectric coefficients, and bulk concentrations. For low salinity, the differential capacitance, as seen in the upper left plot of Figure 4.7, decreases substantially as the size of couterion increases; however, it does not have noticeable change for the positive potential when the size of coions increases. This again illustrates that our model can effectively capture the effect of non-uniform ionic sizes. It is interesting to notice that the surface potential corresponding to peaks decreases as counterion size increases, because a lower surface potential is needed to trigger counterion saturation when counterion size is large. To study the effect of dielectric coefficient of counterions, we fix the counterion volume ($v_1 = 0.662^3\,\mathrm{nm}^3$) as well as other parameters, and gradually increase the dielectric coefficient from 5 to 30. Since $\varepsilon_1 < \frac{2}{5}\varepsilon_w$ in such cases, the saturation due to dielectric decrement prevails the size-effect saturation. As shown in the upper right plot of Figure 4.7, the differential capacitance enhances as the dielectric coefficient of counterions increases. Also, the surface potential corresponding to peaks decreases, as the counterion saturation occurs at a lower surface potential for a smaller dielectric coefficient. It is of importance to note that the differential capacitance is independent of the dielectric coefficient of coions, indicating that the Bruggeman model indeed predicts an effective dielectric coefficient that reflects different mixture components.

For high salinity, the capacitance-potential curves become a bell shape with a single peak, as discussed in the previous section. As the cation volume increases, the differential capacitance moves down, especially for the positive potential. Notice that the curves become more and more asymmetric as v_1 decreases. With smaller v_1, more ions are able to be attracted to the EDL capacitor when the negatively stronger surface is applied. However, the differential capacitance decreases monotonically for all v_1 when the positively stronger potential is applied. Because, at high salinity, the effective width of EDL grows with positively larger surface potential, no matter how the (coion) size v_1 changes.

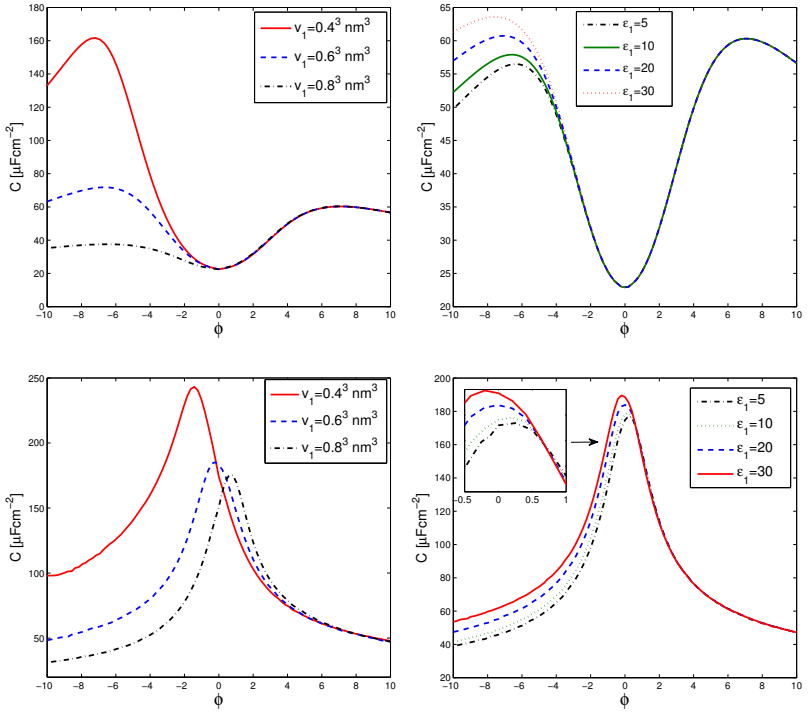

FIG. 4.7. *Differential capacitance versus surface potential using different ionic sizes and dielectric coefficients of hydrated ions. Top: Low salinity* $c_i^\infty = 10mM$*; Bottom: High salinity* ($c_i^\infty = 1M$)*. Left: The cation takes a fixed dielectric coefficient* $\varepsilon_1 = 10$ *but various ionic volumes:* $v_1 = 0.4^3\,nm^3$, $0.6^3\,nm^3$, *and* $0.8^3\,nm^3$*. Right: The cation takes a fixed ionic volume* $v_1 = 0.662^3\,nm^3$ *but various dielectric coefficients:* $\varepsilon_1 = 5$, 10, 20, *and* 30.

As shown in the right plot of Figure 4.7, the variation of dielectric coefficient of ε_1 has some impact on the capacitance-potential curve as well. With larger ε_1, the location of the peak of bell shape curve gradually shifts to negative surface potentials, and the height of the peak increases as well. As ε_1 increases, the dielectric depletion effect diminishes, leading to more ions stored in the EDL capacitor. Further, one can observe that the positive-potential branch of the curves overlap each other, since not many coions are present in the EDL. This again illustrates that our model is capable of capturing the dielectric effect of hydrated ions as a source of ion-specificity.

4.4. Charged cylinders. We investigate the effect of concentration-dependent dielectrics on the electrostatics between two long charged cylinders immersed in a monovalent electrolyte solution. We assume the system is homogeneous along the direction of cylinders; therefore, the system under consideration reduces to a two-dimensional case. The computational domain $[-5,5]\times[-5,5]$ (in nm) is resolved by a 100×100 mesh. The two cylinders of radius 1 nm located at $(-2,0)$ and $(2,0)$ carrying positive charges in the center [24]. The dielectric coefficient in the cylinders is denoted by ε_{int}. The parameters of water molecules and ions are given by

$$\begin{aligned}
&\varepsilon_0 = 78.3, v_0 = 0.275^3\text{nm}^3,\ c_1^\infty = c_2^\infty = 0.1M,\\
&\varepsilon_1 = 46,\quad v_1 = 0.716^3\text{nm}^3,\quad z_1 = +1,\\
&\varepsilon_2 = 12,\quad v_2 = 0.676^3\text{nm}^3,\quad z_2 = -1.
\end{aligned}$$

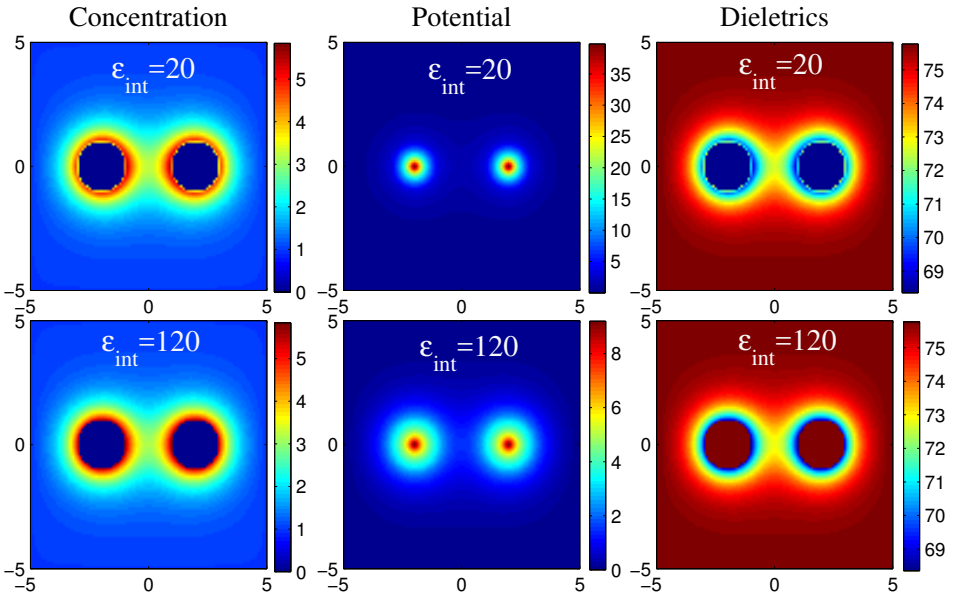

FIG. 4.8. *The equilibrium distribution of counterion concentration, electrostatic potential, and dielectrics with* $\varepsilon_{\text{int}} = 20$ *and* $\varepsilon_{\text{int}} = 120$.

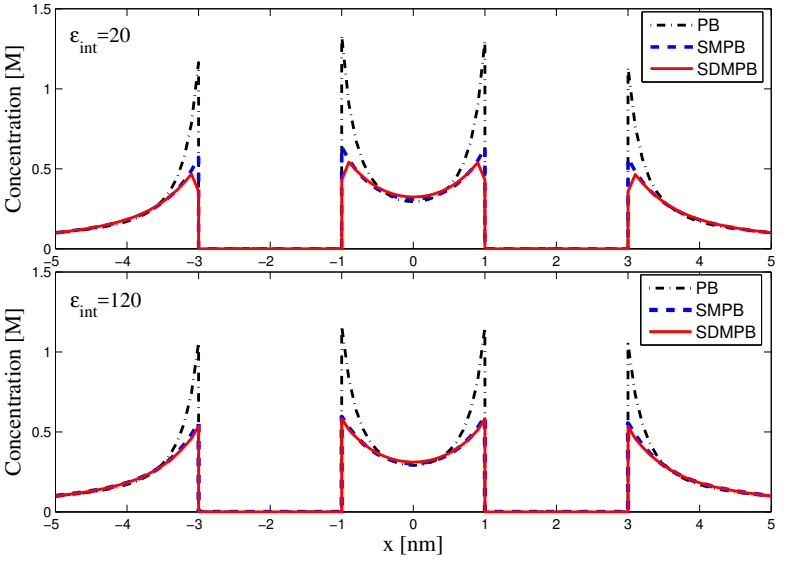

FIG. 4.9. *Counterion concentration predicted by the PB, SMPB, and SDMPB models along the x-axis with* $\varepsilon_{\text{int}} = 20$ *and* $\varepsilon_{\text{int}} = 120$.

To explore the impact of dielectric coefficient of cylinders, we perform numerical simulations with $\varepsilon_{\text{int}} = 20$ and $\varepsilon_{\text{int}} = 120$. Figure 4.8 displays the equilibrium distribution of counterion concentrations, electrostatic potential, and dielectrics with low and high dielectric coefficients in the cylinders. As expected, the counterions are attracted to charged cylinders. High concentration leads to dielectric decrement around the cylin-

ders. Due to the effect of dielectric depletion, the counterion concentration in the close vicinity of cylinders is lowered for the case of $\varepsilon_{\text{int}} = 20$. Correspondingly, the electrostatic potential is much higher because it is less screened by the lower dielectric profile.

For comparison, we also perform simulations with the classical PB and SMPB models, in which the dielectric coefficient outside the cylinders takes $\varepsilon = \varepsilon_w$. To have a quantitative comparison, we show in Figure 4.9 the counterion concentration predicted by the PB, SMPB, and SDMPB models along the x-axis. Clearly, the classical PB model that ignores steric effects predicts high concentration around the cylinders. In comparison with SMPB, our SDMPB model predicts a bit lower counterion concentration with $\varepsilon_{\text{int}} = 20$ because of dielectric depletion. For the case of $\varepsilon_{\text{int}} = 120$, the dielectric depletion is suppressed by large dielectric coefficient inside the cylinders — the SDMPB predicts slightly lower counterion concentration than that of the SMPB model.

5. Conclusions

In this work, we develop a modified Poisson–Boltzmann (PB) theory with a variational approach that takes the nonlinear concentration-dependent dielectrics into account. The effective dielectric coefficient, as a nonlinear implicit function on both counterion and coion concentrations, is determined by solving the Bruggeman equation, which provides a closure to the modified PB theory. In addition to ionic size and valence, our theory introduces a new source of ion-specificity, i.e., the dielectric coefficient of hydrated ions, to the continuum modeling of electrostatics. Robust and efficient numerical methods with acceleration techniques are proposed for solving the equilibrium state of the PB theory.

We further analyze the Bruggeman model in the limits of dilute and concentrated concentrations. The connection between the Bruggeman model and previous linear decrement models is established via asymptotic expansions. Also, we derive a modified Grahame equation that relates the surface charge density, effective dielectric coefficient, and ionic concentrations at a charged surface. Such a relation leads to a saturation concentration of counterions due to dielectric decrement. Furthermore, we investigate the counterion saturation arising from both the steric effects and dielectric decrement. A criterion has been derived to tell which of the two will become predominant in determining counterion distribution. The criterion has been confirmed later by numerical simulations.

We apply the modified PB theory to study dielectrics of electrolytes. The prediction by our model has good agreement with experimental data. The dielectric decrement effect on the structure of the electric double layer (EDL) has been extensively assessed with numerical simulations. We also apply the developed modified PB theory to study the differential capacitance of the EDL capacitors. The profound effect of counterion saturation, due to steric effects and dielectric decrement, on the shape of differential capacitance profiles is theoretically analyzed and numerically investigated. With ion-specific parameters, our theory is able to reproduce asymmetric camel-shape profiles of differential capacitance against applied potentials for electrolytes with low salinity, and asymmetric bell-shape profiles for electrolytes with high salinity. The newly introduced dielectric coefficients of hydrated ions provide a new perspective to study the asymmetry of differential capacitance profiles. The modified PB theory is also applied to probe the effect of concentration-dependent dielectrics on electrostatics between two charged cylinders with various dielectric constants.

We now discuss several issues and possible further refinements of our work. Continuum dynamical models, such as the modified Poisson–Nernst–Planck equations with the Bruggeman equation, can be readily derived from the electrostatic free-energy func-

tional. It is of significance to assess the effect of concentration-dependent dielectrics on ionic transport in ion channels, nanofluidic devices, and electrochemical systems [56]. Our analysis on the Bruggeman equation shows that the Hessian matrix of the function of effective dielectric coefficient on concentrations is indefinite. As analyzed in our previous work [33], the electrostatic free-energy functional may be nonconvex with respect to concentrations. It remains for future work to study the existence of multiple equilibrium solutions that are of physical interest, and to perform stability analysis on the multiple solutions in dynamical models. The effective dielectric coefficient, determined by the Bruggeman equation, is a spatially inhomogeneous function of concentrations. To account for dielectric inhomogeneity, the Born energy of solvated ions can be taken into account [37, 49]. The impact of Born energy on the structure of EDLs and the differential capacitance of EDL capacitors deserves further studies.

Acknowledgments. This work is supported by the grants NSFC 11601361 and 21773165, Natural Science Foundation of Jiangsu Province, China (BK20160302), and Soochow University Q410700415. The authors thank anonymous referees for their valuable comments.

REFERENCES

[1] R. Adams, *Sobolev Spaces*, Academic Press, New York, 1975. 2.1
[2] M. Bazant, B. Storey, and A. Kornyshev, *Double layer in ionic liquids: Overscreening versus crowding*, Phys. Rev. Lett., 106:046102, 2011. 1
[3] M.Z. Bazant, M.S. Kilic, B.D. Storey, and A. Ajdari, *Towards an understanding of induced-charge electrokinetics at large applied voltages in concentrated solutions*, Adv. Colloid. Interface Sci., 152:48–88, 2009. 4.3.1, 4.3.1
[4] D. Ben-Yaakov, D. Andelman, D. Harries, and R. Podgornik, *Beyond standard Poisson–Boltzmann theory: Ion-specific interactions in aqueous solutions*, J. Phys. Condens. Matter, 21:424106, 2009. 1, 2.4, 2
[5] D. Ben-Yaakov, D. Andelman, and R. Podgornik, *Dielectric decrement as a source of ion-specific effects*, J. Chem. Phys., 134:074705, 2011. 1, 1, 2.4, 4.2
[6] R. Bikky, N. Badi, and A. Bensaoula, *Effective medium theory of nanodielectrics for embedded energy storage capacitors*, Proceedings of the COMSOL Conference, Boston, 2010. 1
[7] I. Borukhov, D. Andelman, and H. Orland, *Steric effects in electrolytes: A modified Poisson–Boltzmann equation*, Phys. Rev. Lett., 79:435–438, 1997. 2.1, 2.4, 2
[8] D.A.G. Bruggeman, *Berechnung verschiedener physikalischer konstanten von heterogenen substanzen. I. Dielektrizittskonstanten und Leitfhigkeiten der Mischkrper aus isotropen substanzen*, Ann. Phys. (Leipzig), 24:636–679, 1935. 1, 2.1
[9] R. Buchner, G.T. Hefter, and J. Barthel, *Dielectric relaxation of aqueous NaF and KF solutions*, J. Chem. Soc. Faraday Trans., 90:2475–2479, 1994. 1, 4.1
[10] H. Chen and A.Z. Panagiotopoulos, *Communication: Modeling electrolyte mixtures with concentration dependent dielectric permittivity*, J. Chem. Phys., 148(4):041102, 2018. 1, 1
[11] M. Davis and J.A. McCammon, *Dielectric boundary smoothing in finite difference solutions of the Poisson equation: An approach to improve accuracy and convergence*, J. Comput. Chem., 12:909–912, 1991. 3.2
[12] B. Eisenberg, Y. Hyon, and C. Liu, *Energy variational analysis EnVarA of ions in water and channels: Field theory for primitive models of complex ionic fluids*, J. Chem. Phys., 133:104104, 2010. 2.1
[13] M.V. Fedorov, N. Georgi, and A.A. Kornyshev, *Double layer in ionic liquids: The nature of the camel shape of capacitance*, Electrochem. Commun., 12:296–299, 2010. 4.3.2
[14] M.V. Fedorov and A.A. Kornyshev, *Ionic liquid near a charged wall: Structure and capacitance of electrical double layer*, J. Phys. Chem. B, 112:11868–11872, 2008. 4.3.2
[15] D. Frydel, *Polarizable Poisson–Boltzmann equation: The study of polarizability effects on the structure of a double layer*, J. Chem. Phys., 134:234704, 2011. 1
[16] N. Gavish, C. Liu, and B. Eisenberg, *Do bistable steric Poisson–Nernst–Planck models describe single-channel gating?* J. Phys. Chem. B, 122(20):5183–5192, 2018. 2.1
[17] N. Gavish and K. Promislow, *Dependence of the dielectric constant of electrolyte solutions on ionic concentration: A microfield approach*, Phys. Rev. E, 94:012611, 2016. 1, 1, 4.1

[18] N. Gavish and K. Promislow, *On the structure of generalized Poisson–Boltzmann equations*, Euro. J. Appl. Math., 27:667–685, 2016. 1
[19] D.C. Grahame, *Differential capacity of mercury in aqueous sodium fluoride solutions. I. Effect of concentration at* 25°, J. Am. Chem. Soc., 76:4819–4823, 1954. 4.3.2
[20] X. Guan, M. Ma, Z. Gan, Z. Xu, and B. Li, *Hybrid Monte Carlo and continuum modeling of electrolyte with concentration-induced dielectric variations*, Phys. Rev. E, 94:053312, 2016. 1, 2.4, 4.2
[21] J.B. Hasted, *Aqueous Dielectrics*, Chapman and Hall, London, 1973. 1, 1, 4.1
[22] J.B. Hasted, D.M. Riston, and C.H. Collie, *Dielectric properties of aqueous ionic solutions. Parts I and II*, J. Chem. Phys., 16:1–21, 1948. 1, 1, 1, 4.1
[23] T. Horng, T. Lin, C. Liu, and R. Eisenberg, *PNP equations with steric effects: a model of ion flow through channels*, J. Phys. Chem. B, 116(37):11422–11441, 2012. 2.1
[24] B. Huang, S. Maset, and K. Bohinc, *Interaction between charged cylinders in electrolyte solution. Excluded volume effect*, J. Phys. Chem. B, 121:9013–9023, 2017. 4.4
[25] Y. Hyon, B. Eisenberg, and C. Liu, *A mathematical model for the hard sphere repulsion in ionic solutions*, Commun. Math. Sci., 9:459–475, 2011. 2.1
[26] J.N. Israelachvili, *Intermolecular and Surface Forces*, Academic Press, Third Edition, 2010. 2.3
[27] D. Jiang, D. Meng, and J. Wu, *Density functional theory for differential capacitance of planar electric double layers in ionic liquids*, Chem. Phys. Lett., 504(4):153–158, 2011. 4.3.2
[28] A.A. Kornyshev, *Double-layer in ionic liquids: Paradigm change?* J. Phys. Chem. B, 111(20):5545–5557, 2007. 2.4, 4.3.1, 4.3.2
[29] R. Landauer, *Electrical conductivity in inhomogeneous media*, AIP Conf. Proc., 40(1):2–45, 1978. 1
[30] A. Levy, D. Andelman, and H. Orland, *Dielectric constant of ionic solutions: A field-theory approach*, Phys. Rev. Lett., 108:227801, 2012. 1, 4.1
[31] B. Li, *Continuum electrostatics for ionic solutions with nonuniform ionic sizes*, Nonlinearity, 22:811–833, 2009. 2.1, 2.4, 2
[32] B. Li, P. Liu, Z. Xu, and S. Zhou, *Ionic size effects: Generalized Boltzmann distributions, counterion stratification, and modified Debye length*, Nonlinearity, 26:2899–2922, 2013. 2.4
[33] B. Li, J. Wen, and S. Zhou, *Mean-field theory and computation of electrostatics with ionic concentration dependent dielectrics*, Commun. Math. Sci., 14:249–271, 2016. 1, 1, 2.2, 2.4, 4.2, 5
[34] H. Li and B. Lu, *An ionic concentration and size dependent dielectric permittivity Poisson–Boltzmann model for biomolecular solvation studies*, J. Chem. Phys., 141:024115, 2014. 1
[35] J. Liu, D. Xie, and B. Eisenberg, *Poisson-Fermi formulation of nonlocal electrostatics in electrolyte solutions*, Mol. Based Math. Biol., 5:116–124, 2017. 2.1
[36] J.-L. Liu and B. Eisenberg, *Poisson-Nernst-Planck-Fermi theory for modeling biological ion channels*, J. Chem. Phys., 141(22):22D532, 2014. 2.1
[37] P. Liu, X. Ji, and Z. Xu, *Modified Poisson–Nernst–Planck model with accurate Coulomb correlation in variable media*, SIAM J. Appl. Math., 78:226–245, 2018. 5
[38] X. Liu, Y. Qiao, and B. Lu, *Analysis of the mean field free energy functional of electrolyte solution with non-homogenous boundary conditions and the generalized PB/PNP equations with inhomogeneous dielectric permittivity*, SIAM J. Appl. Math., 78:1131–1154, 2018. 2.1
[39] M. Ma and Z. Xu, *Self-consistent field model for strong electrostatic correlations and inhomogeneous dielectric media*, J. Chem. Phys., 141:244903, 2014. 1
[40] M. Ma, S. Zhao, and Z. Xu, *Investigation of dielectric decrement and correlation effects on electric double-layer capacitance by self-consistent field model*, Comm. Comput. Phys., 20:441–458, 2016. 1
[41] Y. Nakayama and D. Andelman, *Differential capacitance of the electric double layer: The interplay between ion finite size and dielectric decrement*, J. Chem. Phys., 42(4):044706, 2015. 1, 1, 2.2, 2.4, 2.4, 4.2, 4.3, 4.3.1, 4.3.2
[42] E.R. Nightingale, *Phenomenological theory of ion solvation. Effective radii of hydrated ions*, J. Phys. Chem., 63:1381–1387, 1959. 4.1
[43] L. Pilon, H. Wang, and A. d'Entremont, *Recent advances in continuum modeling of interfacial and transport phenomena in electric double layer capacitors*, J. Electrochem. Soc., 162(5):A5158–A5178, 2015. 4.3.1
[44] F. Siddiqua, Z. Wang, and S. Zhou, *A modified Poisson–Nernst–Planck model with excluded volume effect: theory and numerical implementation*, Commun. Math. Sci., 16(1):251–271, 2018. 2.1
[45] J. Sin, *Influence of solvent polarization and non-uniform ion size on electrostatic properties between charged surfaces in an electrolyte solution*, J. Chem. Phys., 147(21):214702, 2017. 1
[46] D. Stroud, *The effective medium approximations: Some recent developments*, Superlattices Mi-

crostruct., 23:567–573, 1998. 1

[47] G. Treset, *Generalized Poisson–Fermi formalism for investigating size correlation effects with multiple ions*, Phys. Rev. E, 78:061506, 2008. 1, 2.1

[48] C. Tuck, *Effective Medium Theory*, Oxford: Clarendon Press, Oxford, First Edition, 1999. 1

[49] Z.G. Wang, *Fluctuation in electrolyte solutions: The self energy*, Phys. Rev. E, 81:021501, 2010. 5

[50] Y. Wei, P. Chiang, and S. Sridhar, *Ion size effects on the dynamic and static dielectric properties of aqueous alkali solutions*, J. Chem. Phys., 96:4569–4573, 1992. 1, 4.1

[51] Y. Wei and S. Sridhar, *Dielectric spectroscopy up to 20 GHz of LiCl/*H_2O *solutions*, J. Chem. Phys., 92:923–926, 1990. 1, 4.1

[52] D. Xie and Y. Jiang, *Nonlocal Poisson-Fermi double-layer models: Effects of nonuniform ion sizes on double-layer structure*, Phys. Rev. E, 97:052610, 2018. 1

[53] D. Xie, Y. Jiang, P. Brune, and L.R. Scott, *A fast solver for a nonlocal dielectric continuum model*, SIAM J. Sci. Comput., 34(2):B107–B126, 2012. 1

[54] D. Xie, J. Liu, and B. Eisenberg, *Nonlocal poisson-fermi model for ionic solvent*, Phys. Rev. E, 94:012114, 2016. 1, 2.1

[55] S. Xu, P. Sheng, and C. Liu, *An energetic variational approach for ion transport*, Commun. Math. Sci., 12:779–789, 2014. 2.1

[56] H. Zhao and S. Zhai, *The influence of dielectric decrement on electrokinetics*, J. Fluids Mech., 724:69–94, 2013. 5

[57] S. Zhou, Z. Wang, and B. Li, *Mean-field description of ionic size effects with non-uniform ionic sizes: A numerical approach*, Phys. Rev. E, 84:021901, 2011. 2.4